Heliyon 9 (2023) e17749

Contents lists available at ScienceDirect

Heliyon

journal homepage: www.cell.com/heliyon

Thermally generated Au–Ag nanostructures with tunable localized surface plasmon resonance as SERS activity substrates

Jialin Ji [a,b,*], Zhengwang Li [b]

[a] Tongda College of Nanjing University of Post and Telecommunications, No. 33 South of Runyang Road, Yangzhou 225127, People's Republic of China

[b] Engineering Research Center of Optical Instrument and System, Ministry of Education and Shanghai Key Lab of Modern Optical System, University of Shanghai for Science and Technology, No. 516 Jun Gong Road, Shanghai 200093, People's Republic of China

ARTICLE INFO

Keywords:
Thermal annealing
Red-shift
Surface-enhanced Raman scattering
Au/Ag bimetallic clusters
Ag–Au core-shell

ABSTRACT

Various Au–Ag bimetallic alloy nanostructures were obtained as sensitive surface-enhanced Raman scattering (SERS) substrates by changing the thermal annealing sequence. The atomic force microscopy (AFM) and scanning electron microscopy (SEM) results confirm that Au/Ag bimetallic clusters and Ag–Au core-shell like structures can be designed by thermal annealing. The absorption spectra showed that the localized surface plasmon resonance (LSPR) frequency of the annealed Au/Ag bimetallic alloy structure could effectively shift from the near ultraviolet to the visible region. At the same time, the Au/Ag bimetallic alloy films modified by thermal annealing have shown satisfactory performance as SERS substrates. Raman enhancement mechanism of Au–Ag bimetallic alloy films is verified by finite-difference time-domain (FDTD) simulation results.

1. Introduction

Surface-enhanced Raman scattering (SERS) has become a powerful analytical technique since its discovery in 1974 [1] and has attracted increasing attention in the chemical and biological detection of low-concentration molecules, DNA, and pathogens [2,3,4]. Due to its molecular fingerprinting capabilities, ultra-high and single-molecular detection sensitivity [5,6,7], non-destructive nature, and real-time label-free analysis, SERS has many valuable applications [8]. However, SERS usually has a weak signal. That is why much research has focused on enhancing the SERS signal and expanding its vast potential for chemical and biomolecular sensing [9,10,11]. Electromagnetic enhancement and chemical enhancement are the two main SERS enhancement mechanisms. Compared to the relatively low efficiency of chemical enhancement, electromagnetic enhancement is very efficient in enhancing SERS, mainly caused by the local plasmon resonance of the sample, with enhancement factors up to 10^{14} [12,13]. The enhancement is highly dependent on the size, shape, and structure of the material used to prepare the substrate. Metal nanostructures with fine-tuning properties of localized surface plasmon resonance (LSPR) have significant applications in surface-enhanced Raman scattering, particularly as substrates for SERS [14].

Typically, nanostructured plasmonic materials such as gold (Au) and silver (Ag) nanoparticles with LSPR frequencies in the visible to the near-infrared range are used for enhancing SERS [15]. However, bimetallic alloy nanoparticles consisting of two different

* Corresponding author. Tongda College of Nanjing University of Post and Telecommunications, No. 33 South of Runyang Road, Yangzhou 225127, People's Republic of China.

E-mail addresses: ji_jia_lin@163.com, 1527930521@qq.com (J. Ji).

https://doi.org/10.1016/j.heliyon.2023.e17749
Received 2 June 2023; Received in revised form 22 June 2023; Accepted 27 June 2023
Available online 28 June 2023
2405-8440/© 2023 The Authors. Published by Elsevier Ltd. This is an open access article under the CC BY-NC-ND license (http://creativecommons.org/licenses/by-nc-nd/4.0/).

metallic elements, like gold and silver, have the properties of both metals and are accompanied by metal-to-metal coupling and are therefore more interesting from a scientific and technical point of view than monometallic nanoparticles. For example, Khlebtsov et al. [16] reported core-shell Au–Ag cuboids and dumbbells with SERS enhancement factors up to 10^6. Li et al. [17] reported SERS applications of alloyed Ag–Au hollow nanocubes with enhanced SERS of 10^7. In contrast to metallic SERS substrates designed and fabricated by traditional electron beam, laser lithography, or other chemical synthesis methods, the work in this article required only physical sputter deposition and annealing treatment at a low temperature. Based on our previous report [18], we found that moderate heat treatments can artificially control the geometrical characteristics of the metallic films. The formation of different nanostructures is feasible with an appropriate choice of film thickness, temperature, and order of thermal annealing.

In this study, Au/Ag bimetallic alloy nanostructures were fabricated as sensitive SERS substrates by a cost-effective and environment-friendly thermal annealing. The results of scanning electron microscopy (SEM) and atomic force microscopy (AFM) clearly show the change process of the surface morphology of Au–Ag bimetallic alloy films before to after thermal annealing. By changing the thermal annealing sequence of Au and Ag layers, we obtained Au/Ag bimetallic clusters and Ag–Au core-shell-like structures. The LSPR frequency of the Au/Ag bimetallic alloy structure can also be effectively tuned by changing the thermal annealing sequence. The article also discusses the SERS performances of Au, Ag and Au/Ag bimetallic alloy films with different sequences of thermal annealing. Finally, the electric field distribution of samples was calculated by finite difference time domain (FDTD) simulation to verify the experimental results.

2. Experiment

Prior to film deposition, each fused silica substrate was ultrasonically cleaned with acetone, ethanol, and deionized water for 20 min and dried with N2 flow.

Au thin films with a thickness of 5 nm were deposited on the substrates from a gold target (99.99%, diameter 50 mm) using magnetron sputtering. The chamber was evacuated to a base pressure of about 5.0×10^{-4} Pa and the molecular pump was adjusted to maintain a working pressure of 0.8 Pa. In the magnetron sputtering deposition system, the DC sputtering voltage and current are adjusted so that the power of the gold target is 70 W. The same method was used to deposit Ag films with a thickness of 10 nm. Next, gold films were deposited on top of silver films to prepare Au/Ag bilayer structure. Then, the as-deposited Au/Ag films were vacuum annealed at a temperature of 300 °C for 10 min. For convenience, the annealed Au/Ag sample was marked annealed Au/Ag. Finally, the annealing sequence was changed so that the 10 nm silver film was annealed first, and then a 5 nm gold film was deposited on top to obtain Au/annealed Ag. A quartz crystal microbalance monitored the thickness of all thin films. To better understand the complete process, a schematic of the experiment is shown in Fig. 1.

The crystal structure of the films was examined with X-ray diffraction (XRD, Bruker AXS/D8 Advance). Using stepwise scanning method, X-ray (Cu Kα radiation): voltage 40 Kv, current 30 Ma; incident wavelength $\lambda = 0.15408$ nm, scanning range 10.000–90.000, scanning mode continuous scanning, scanning speed 2.0000deg/min.

The surface roughness was examined with an atomic force microscope (AFM, XE-100, Park Systems). The surface morphology was studied by scanning electron microscopy using a Hitachi S-4800 operating at 10 kV. The measurements were conducted at 5×10^{-4} Pa. The surface roughness was examined with scanning area for 3×3 μm^2.

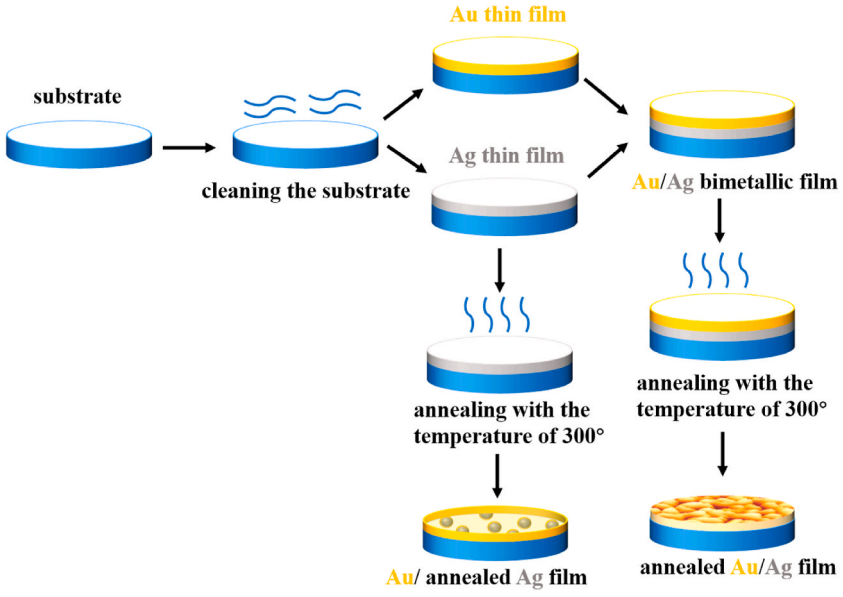

Fig. 1. A schematic diagram of the experimental process.

Optical scattering and absorption in the films were measured with a UV–Vis–NIR double-beam spectrophotometer (Lambda 1050, Perkins Elmer). In this experiment, an integrating sphere accessory was used. The integrating sphere has a wavelength range of 200–1000 nm and is used to measure absorbance with a scan step of 2 nm. The angle of incidence is 0° , and the integration time is 0.24s. The integrating sphere is measured in two modes and the output of the absorption spectrum is performed in reflection mode.

The composition of the samples was measured by X-ray photoelectron spectroscopy (XPS). XPS measurements were performed on a Thermo Scientific Escalab 250Xi with Al Kα excitation source (1486.6 eV) with a 500 μm spot, a full spectrum through energy of 150 eV in steps of 1.0 eV and a narrow spectrum through energy of 30 eV in steps of 0.05 eV. XPS data calibration with conventional exotic adsorbed contaminated carbon (C–C, calibrated to 284.8 eV).

Raman scattering spectra were collected with a confocal microprobe Raman system (LabRAM Aramis, France) and a He–Na laser (473 nm). Its light spot diameter is about 1 μm. All the measurements were carried out at room temperature.

3. Results and discussion

3.1. Structural properties

As shown in Fig. 2, the XRD patterns show the influence of thermal annealing on the structures of Au, Ag, and Au/Ag bimetallic alloy films with different thermal annealing sequences. For the single layer Au film, the preferred orientation at about 38.6 of 2 theta (θ) value corresponds to the Au (111) plane, as confirmed by the standard (JCPDS:04–0784). The gold grains have a preferential orientation along the (111) crystal direction. In general, for non-epitaxial deposition, the film structure tends to be along the (111) or (001) planes due to the minimum surface free energy [19,20]. No prominent peaks corresponding to the single silver film were observed, probably due to the amorphous nature of thin film due to the magnetron sputtering method. The diffraction peak intensity of as-deposited Au/Ag (blue line in Fig. 2) is therefore almost identical to that of Au (black line in Fig. 2).

After modification by thermal annealing, the diffraction peaks of annealed Au/Ag sample are significantly sharper and stronger. The observed increase in the crystallinity could be attributed to the thermal treatment that can restore structural defects [21,22,23]. Meanwhile, a weaker secondary diffraction peak is observed at 2θ of around 44.2°, which is the (200) plane of Ag. It is proved that the fabrication of the alloy film has been completed. Moreover, it should be noted that the annealing sequence is changed, which means the Ag layer was annealed first, the intensity of the diffraction peaks is also higher than that of the as-deposited films. These results reveal that the thermal annealing has a pronounced effect on the grain growth of Au/Ag bilayer thin films.

3.2. Composition and valence state

XPS analysis was performed on the experimental samples of Au/Ag bilayers to confirm that the composition of the bilayers before and after heat treatment were indeed gold and silver. The results are shown in Fig. 3 (a), all three sets of alloy samples show characteristic peaks of O 1s, Au 4f and Ag 3d. The O 1s peak is located near 530 eV and the main components are SiO_2 from the uncovered silica substrate and adsorbed oxygen and/or hydroxyl groups.

As shown in Fig. 3(b) and (c), the binding energies of the peaks centered at 367.7 eV and 373.7 eV correspond to the characteristic peaks of Ag $3d_{5/2}$ and Ag $3d_{3/2}$, respectively, and the characteristic peaks of Au $4f_{5/2}$ and Au $4f_{7/2}$ located at 87.3 eV and 83.6 eV, respectively, which are similar to those reported in the literatures [24,25]. After annealing, we can find that there are some negative shifts in the binding energies of Ag and Au element of annealed Au/Ag and the Au/annealed Ag samples. The decrease in binding energy in the annealed samples confirms the increase in electron density on the surface of the Au–Ag alloy, indicating the existence of electron transfer at the contact surface of gold and silver, further demonstrating the formation of a bimetallic alloy structure. This

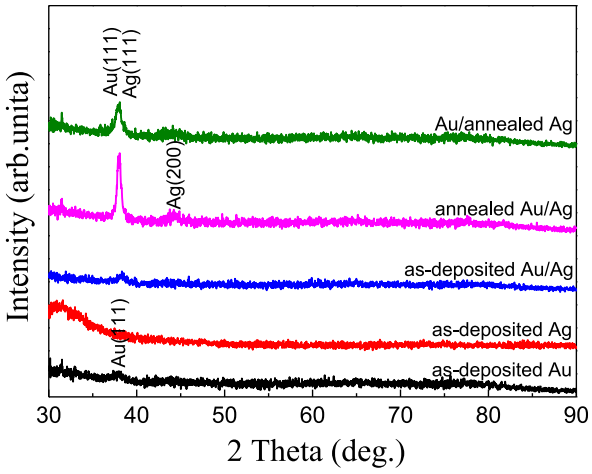

Fig. 2. XRD pattern of Au, Ag, and Au/Ag bimetallic alloy films with different thermal annealing sequences.

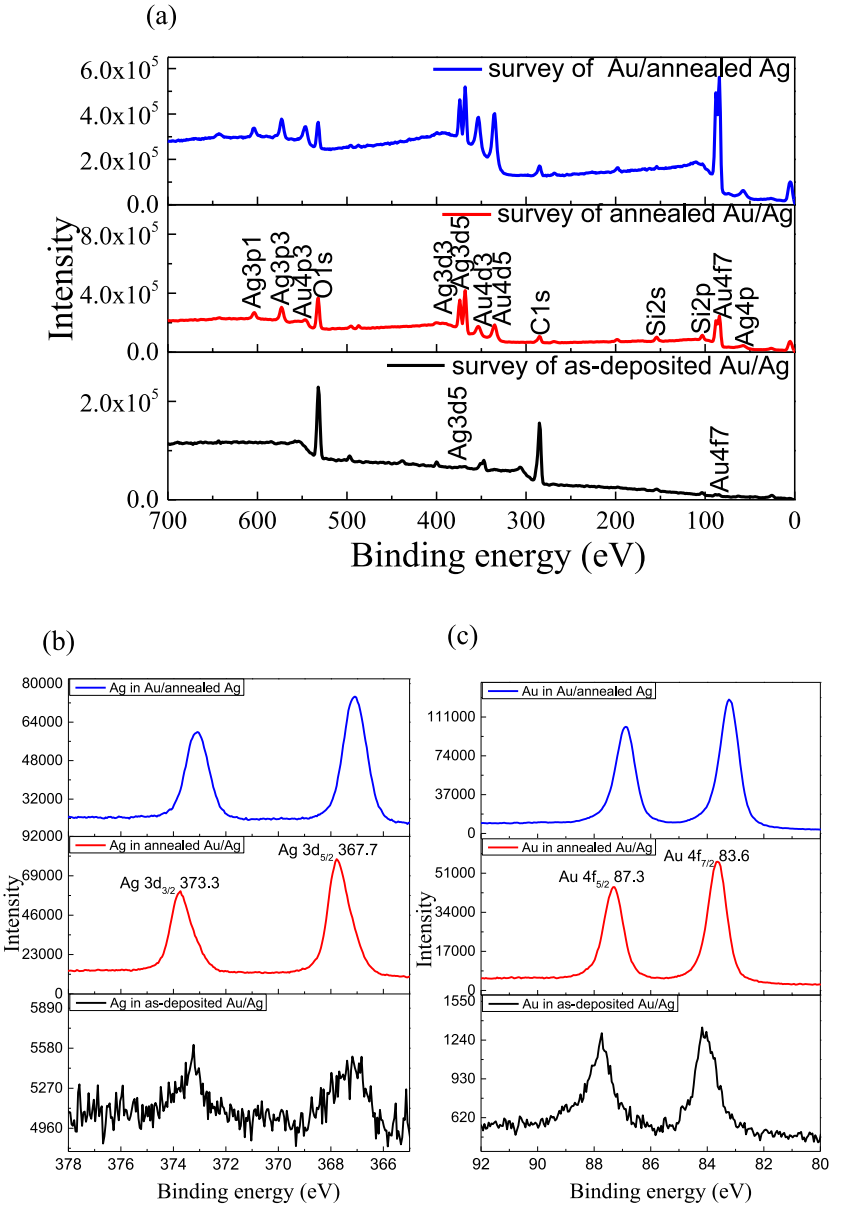

Fig. 3. (a)The XPS spectra of as-deposited Au/Ag bilayer alloy film, the annealed Au/Ag sample, and the Au/annealed Ag sample. (b) Ag element spectra of as-deposited Au/Ag, annealed Au/Ag, and the Au/annealed Au samples; (c) Ag element spectra of as-deposited Au/Ag, annealed Au/Ag, and the Au/annealed Ag samples.

result has a positive impact on the subsequent SPR.

3.3. Surface morphology

Fig. 4 shows the SEM images of the Au, Ag, and Au/Ag bimetallic alloy films with different thermal annealing sequences. It is seen that thermal annealing has a vital influence on the morphology of the materials. Fig. 4(a–c) presents the SEM images of the deposited Au, Ag, and Au/Ag bilayer alloy films. The surface morphologies of the deposited thin films are similar, showing a continuous structure with no visible particles observed on them. However, as the Au/Ag bilayer alloy film was thermally annealed, the heat energy was transferred to the surfaces. That is why this film has discontinuities and nanoparticles with numerous air slits, gaps, or holes at the nanometer scale, which eventually led to a cluster structure [26,27], as shown in Fig. 4(d).

In our previous study [18], when the annealing sequence was changed, the lower layer Ag film was first transformed into ellipsoid Ag nanoparticles (NPs), as shown in the inset of Fig. 4(e), in a vacuum chamber at 300 °C for 10 min. Then, a thin Au layer was put on

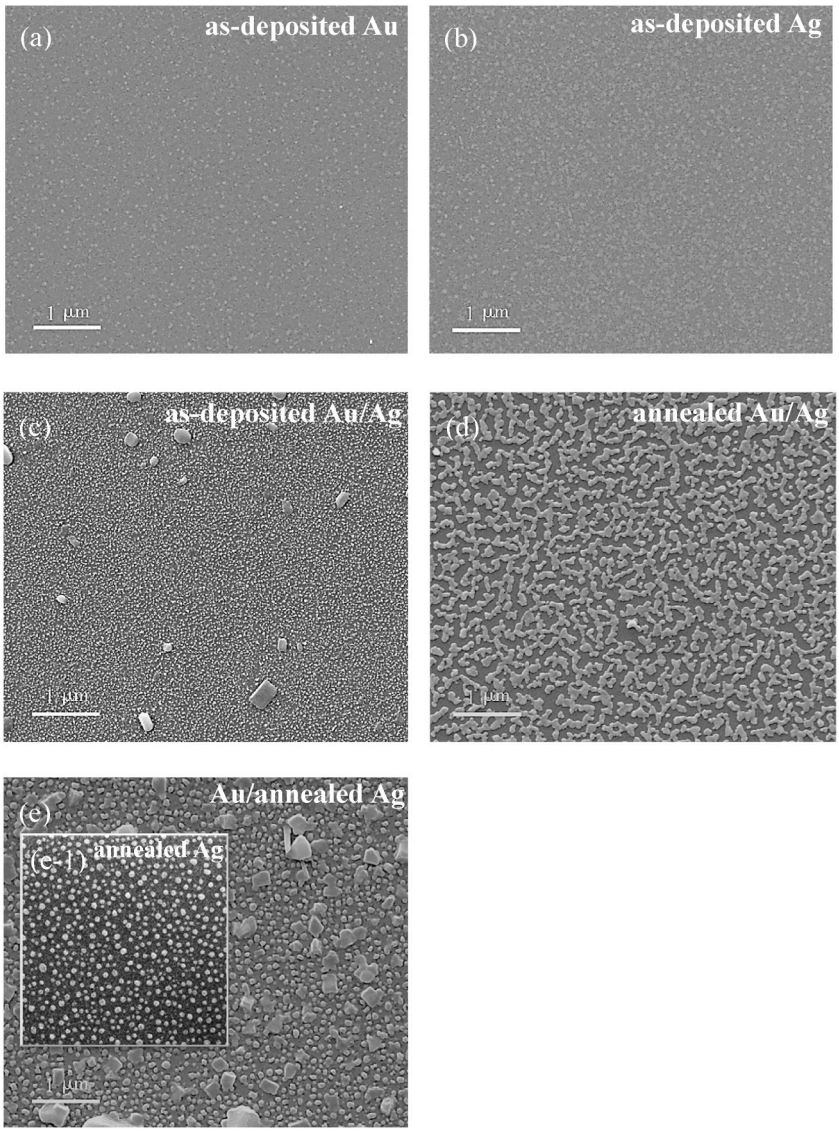

Fig. 4. SEM images of (a) as-deposited Au film, (b) as-deposited Ag film, (c) as-deposited Au/Ag bilayer alloy film. (d) The annealed Au/Ag clusters, and (e) the Ag/Au core–shell-like nanoparticles, in which the silver was first annealed into Ag nanoparticles as shown in the inset (e−1).

the top, the Au film grows along the surface of the Ag nanoparticles and the film transformed into Ag/Au core–shell-like nanoparticles, as shown in Fig. 4(e). These metallic nanostructures positively impact the SERS properties of the samples.

Fig. 5 shows the AFM images of Au, Ag, and Au/Ag bimetallic alloy films with different thermal annealing sequences for a scan area of $3 \times 3\ \mu m^2$. For the deposited Au, Ag, and Au/Ag bimetallic films, as shown in Fig. 5(a–c), the morphologies of the deposited samples are continuous with smooth surfaces. Under the effect of thermal annealing, as shown in Fig. 5(e–f), the surface morphologies of the Au/Ag films were transformed into discontinuous nanostructures, and the surface roughness subsequently increased. As shown in Fig. 5(f), the RMS surface roughness values of the Au, Ag, as-deposited Au/Ag, annealed Au/Ag, and Au/annealed Ag samples are 3.53, 4.52, 5.42, 6.54, and 8.54 nm, respectively. These results are also consistent with the SEM results.

3.4. Optical absorption

Fig. 6 (a) shows the absorption spectra of Au, Ag, and Au/Ag bimetallic alloy films with different thermal annealing sequences. A wave crest for the wavelength corresponding to the maximum absorption in each absorption spectrum is shown in Fig. 6 (b). Fig. 6(c) shows the films without annealing treatment, only one LSPR) peak occurs at around 500 nm for a single Au film [28]. Similarly, for pure silver film, only one LSPR peak occurs at around 320 nm [29]. When the Au is deposited on the Ag layer, the Au/Ag bimetallic film exhibits a broad Ag-like LSPR peak located between the LSPR peaks of the two monometallic plasma edges of Ag (with LSPR peak at

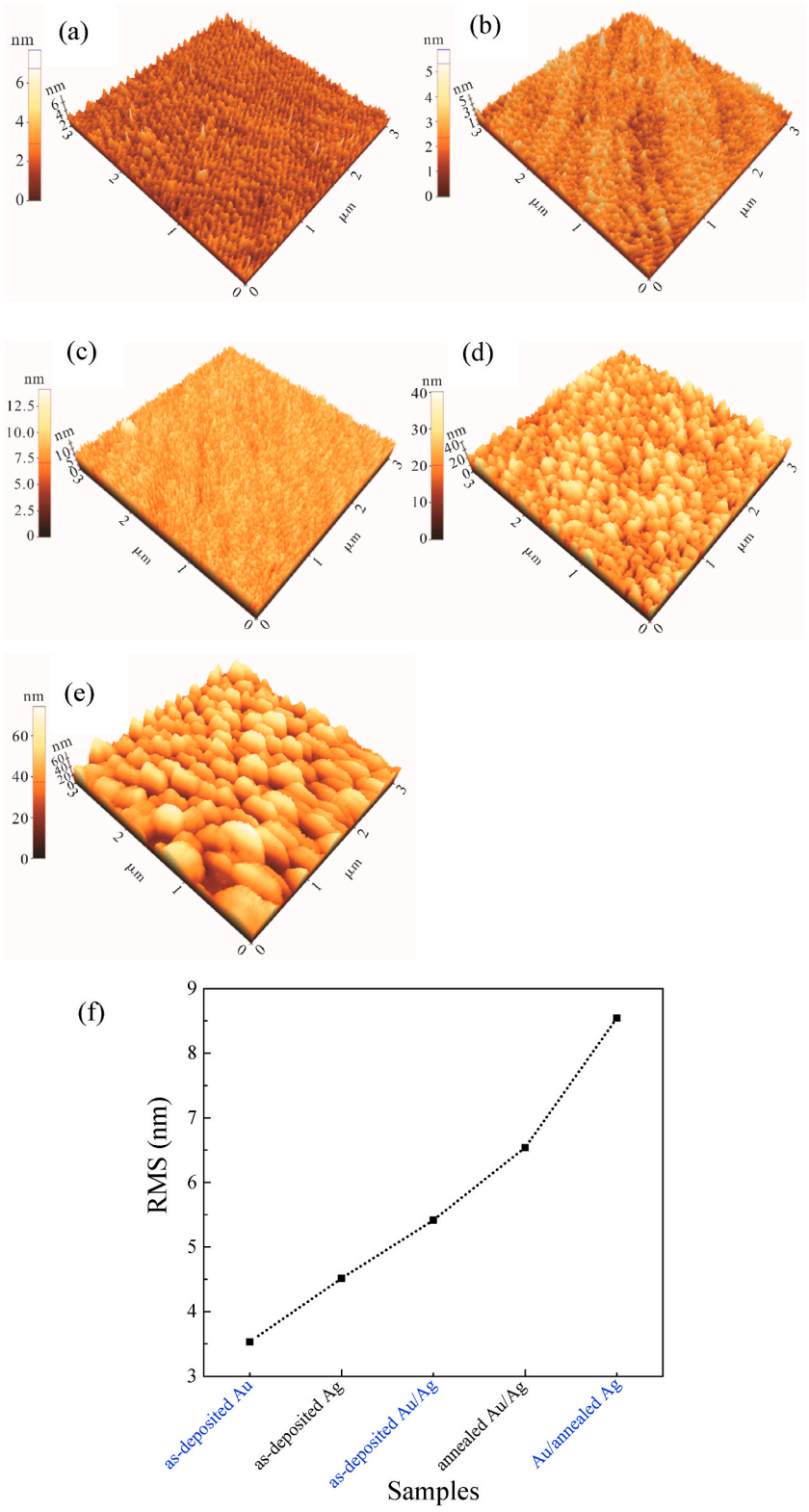

Fig. 5. AFM images of (a) as-deposited Au film, (b) as-deposited Ag film, (c) as-deposited Au/Ag bilayer alloy film. (d) The annealed Au/Ag clusters, (e) the Ag/Au core–shell-like nanoparticles, and (f) the root-mean-square (RMS) surface roughness values of images in (a)–(e).

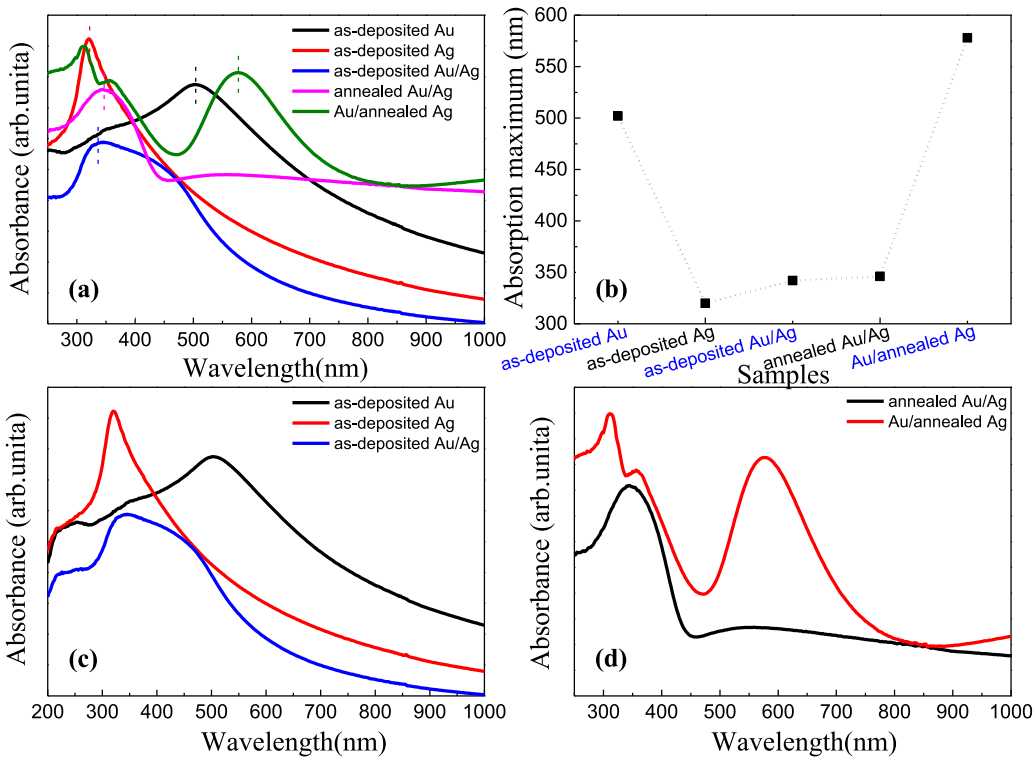

Fig. 6. (a) Absorption spectra of Au, Ag, and Au/Ag bimetallic alloy films with different thermal annealing sequences. (b) Curve of wave crests from every absorption spectrum. (c) Absorption spectra of the deposited Au, Ag, and Au/Ag films and (d) absorption spectra of Au/Ag alloy films under a tuned thermal annealing order.

320 nm) and Au (with LSPR peak at 500 nm). It suggests that gold and silver metals determine these alloy films' optical properties [30]. This result differs from the mono-metal alone and suggests that the bimetal Ag–Au film has been formed, its occurrence leads to a broad-peak absorption band. However, after the thermal annealing, for the annealed Au/Ag sample, the resonance absorption shifts to a longer wavelength with a sharp peak. This phenomenon can be explained by the change in surface morphology of the Au/Ag alloy films. As seen in the SEM (Fig. 4 (a)–(d)) images, the annealed Au/Ag cluster produces a stronger resonant frequency, which results in a red shift with a sharp relative to the initially deposited Au/Ag sample [31].

Fig. 6(d) shows the absorption spectra for Au/Ag alloy films under a tuned thermal annealing order. The absorption profile of the Au/annealed Ag film (red curve in Fig. 6(d)) is entirely different from that of the annealed Au/Ag film (black curve in Fig. 6(d)). It indicates that the Au film occurs on the surface of the preformed Ag core rather than forming more nucleation sites. Moreover, it also shows that the core-shell like structure of the Au–Ag alloy nanoparticles has been formed [32,33,34]. The LSPR wavelength of Au/annealed Ag film is further red-shifted to 578 nm with a stronger LSPR peak in the longer wavelength [35]. On the one hand, this is because the contact surface coupling of the silver nanoparticles with the gold film and excite more LSPR. while on the other hand, it is because the size and spacing of the silver NPs wrapped by the gold layer further increase after the first annealing of the silver. It is well known that the wavelength of the plasma strongly depends on the size of NPs [36]. The AFM and SEM results are evidence of producing an Ag/Au core–shell-like structure with larger metal nanoparticles, resulting in the broader plasmon resonance spectrum and more substantial optical field coupling effects. Therefore, the LSPR is strong and red-shifted. These results show that tuning the LSPR by adjusting the heat treatment sequence of the Au–Ag bimetallic films is an effective method.

3.5. SERS performance

To demonstrate the potential application of tunable LSPR absorption, the Au, Ag, as-deposited Au/Ag, annealed Au/Ag, and Au/annealed Ag samples were used as SERS substrates for probing a specific artificial dye Rhodamine B (Rh B) molecules having concentration $= 1 \times 10^{-4}$ M. For comparison, the Raman intensity of Rh B films is shown in Fig. 7(a).

As shown in Fig. 7(b), the monolayer of Au film deposited on silica shows a Raman spectrum (green line) having very low-intensity peaks. These low-intensity peaks of the Raman spectrum indicate that the Au nanoparticle substrate is inactive for SERS. The silver film substrate is active for SERS. Therefore, the silver film substrate provides strong resonance absorption and low optical loss, making the SERS signal intensity extraordinarily strong. However, the Au/Ag bimetallic film shows a Raman spectrum (blue line in Fig. 7(b)) that is worse than the pure silver film but better than the gold film.

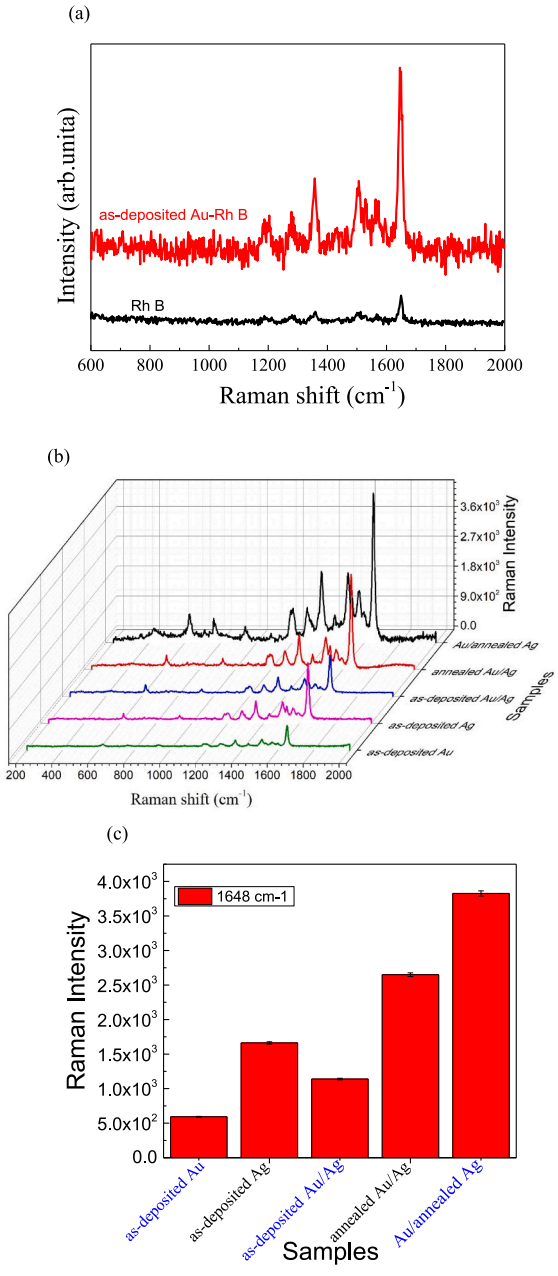

Fig. 7. Raman scattering spectra of (a)Rh. B and it on Au. (b) Raman scattering spectra of Rh. B on Au, Ag, and Au/Ag bimetallic alloy films with different thermal annealing sequences. (c) the corresponding histogram of Raman intensities of all samples.

After thermal annealing, annealed Au/Ag films show a stronger Raman intensity than deposited Au/Ag films. Such a strong Raman intensity can be attributed entirely to the roughness of the annealed Au/Ag film surface. With thermal annealing, the smooth surface of the sample becomes rougher and more structured, causing more tips or "hot spots" to excite the local electrical fields. It eventually increases the Raman intensity [37]. The Raman intensity is further increased by changing the annealing sequence. Annealing the Ag layer first before depositing the Au film on top of it is an example of changing the annealing sequence. The annealed Ag/Au core–-shell-like nanoparticles with high-density plasmonic "hot spots" and strong plasmon near-field coupling detects the Raman scattering more efficiently. In addition, Fig. 7 (c) shows the corresponding histogram for the intensity variation of the spectra at the Raman shift of 1648 cm^{-1} in Fig. 7(b). These results show that Au/Ag bimetallic alloy films modified by thermal annealing positively affect SERS performance. The Au/annealed Ag film with Ag–Ag core-shell like structure showing the strongest SERS signal for RhB of all samples.

To further verify the electric field enhancement mechanism of the metallic films, the electric field distributions of all samples were

calculated using the FDTD simulations. In the model simulation, plane light was incident on the surface of the structure along the Z-direction, the incident wavelength was 633 nm, and the thicknesses and structures of the Au and Ag films were consistent with the experimental values. Fig. 8 shows the electric field intensity distributions of Au, Ag, and Au/Ag bimetallic alloy films with different thermal annealing sequences. A red spot on the local surface of the image represents tip or "hot spot", indicating the Raman signal of the corresponding film. As shown in Fig. 8(a–b), the electric field strength of the silver film is stronger than that of the gold film, with the strongest electric field strength of 1.9. The electric field strength on the surface of the Au/Ag bimetallic film does not change much, as shown in Fig. 8 (c). However, for the annealed Au/Ag alloy clusters and Ag/Au core-shell-like nanoparticles, the local electric field intensity increases from 4.9 to 7 (Fig. 8(d–e)) due to the increased surface roughness of the structured films and "hot spots". The FDTD simulation results show that the rough and structured Au/Ag bimetallic films after the thermal annealing treatment can effectively enhance the local electric field of the samples. In general, the FDTD simulation results agree with the experimental SERS results.

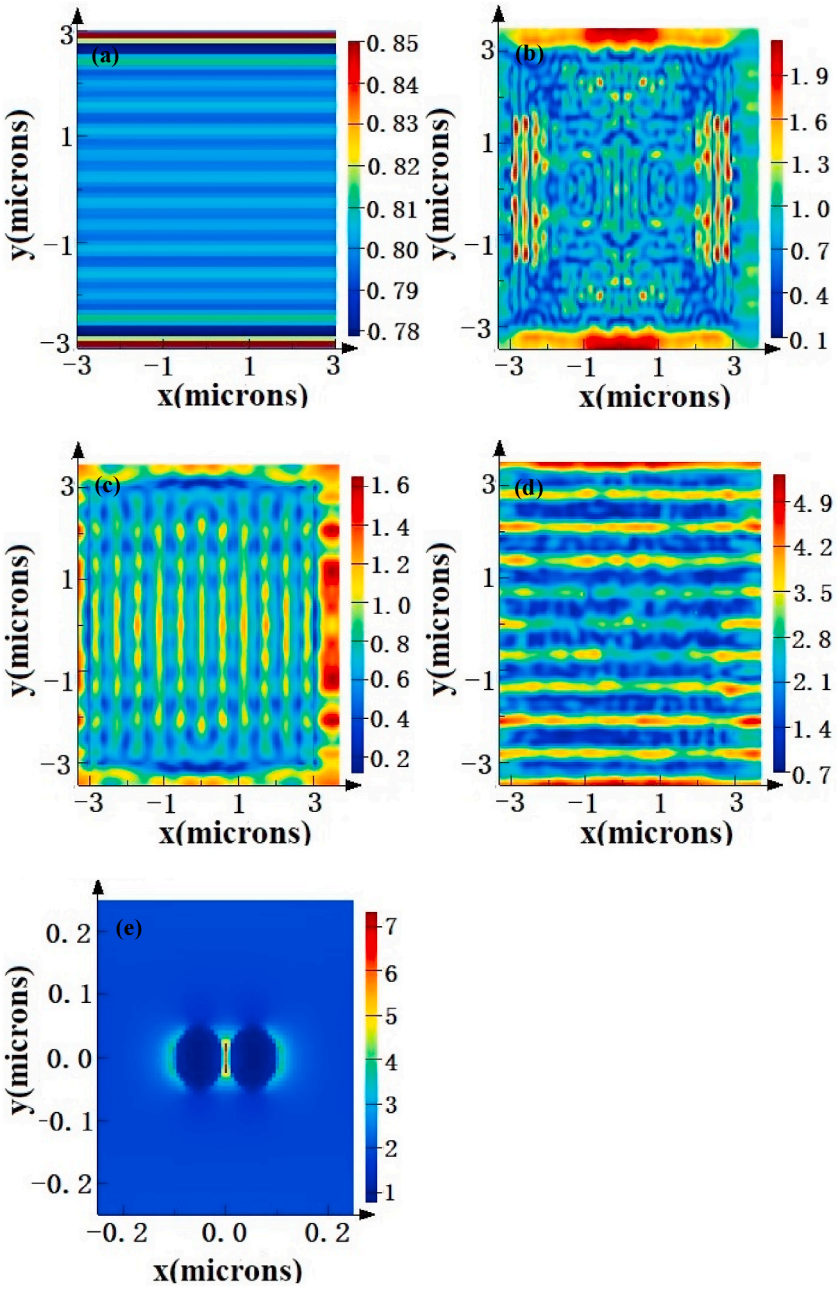

Fig. 8. The simulated electric field strengths at (a) Au film, (b)Ag film, and (c) deposited Au/Ag bilayer alloy film. (d) annealed Au/Ag clusters, and (e) Ag/Au core–shell-like nanoparticles.

4. Conclusions

In summary, we have employed a cost-effective and environment-friendly thermal annealing technique to prepare Au/Ag bimetallic alloy nanostructure substrates for SERS. SEM and AFM results show that various Au/Ag bimetallic alloy nanostructures with rougher surfaces can be obtained by varying the thermal annealing sequence. This variation in the thermal annealing sequence positively influences the SERS performance of the samples. The Au/annealed Ag film shows the strongest SERS signal for RhB of all samples. It indicates the enhancement of the electric field induced by the interfacial coupling between the LSPR effect of Ag nanoparticles and Au film in an Ag–Au core-shell-like structure. FDTD simulations confirmed the SERS enhancement mechanism. Furthermore, the absorption spectra illustrate that the LSPR frequency of the Au/Ag bimetallic alloy structure can be effectively red-shifted from 320 nm to 578 nm after the thermal annealing treatment. These findings open up many opportunities for realizing plasma materials suitable for LSPR sensing, especially as SERS substrates in biosensing applications.

Author contribution statement

Jialin Ji: Conceived and designed the experiments; Performed the experiments; Analyzed and interpreted the data; Wrote the paper.
Zhengwang Li: Contributed reagents, materials, analysis tools or data.

Data availability statement

No data was used for the research described in the article.

Declaration of competing interest

The authors declare that they have no known competing financial interests or personal relationships that could have appeared to influence the work reported in this paper.

Acknowledgments

This work was partially supported by Natural Science Foundation of Jiangsu Province, China (21KJD140004), and Qinglan Project of Jiangsu Province of China, China (QL20221002).

Appendix A. Supplementary data

Supplementary data to this article can be found online at https://doi.org/10.1016/j.heliyon.2023.e17749.

References

[1] M.P. Fleischmann, P.J. Hendra, A.J. Mcquillan, Raman spectra of pyridine adsorbed at a silver electrode, Chem. Phys. Lett. 26 2 (1974) 163–166.
[2] C. Fang, A.V. Ellis, N.H. Voelcker, Electrochemical synthesis of silver oxide nanowires, microplatelets and application as SERS substrate precursors, Electrochim. Acta 59 (2012) 346–353, none.
[3] G. Braun, S.J. Lee, M. Dante, T.Q. Nguyen, N. Reich, Surface-enhanced Raman spectroscopy for DNA detection by nanoparticle assembly onto smooth metal films, J. Am. Chem. Soc. 129 20 (2007) 6378–6379.
[4] A.E. Grow, L.L. Wood, J.L. Claycomb, New biochip technology for label free detection of pathogens and their toxins, J. Microbiol. Methods 53 (2003) 221–233.
[5] H. Xu, E.J. Bjerneld, M. Käll, L. Börjesson, Spectroscopy of single hemoglobin molecules by surface enhanced Raman scattering, Phys. Rev. Lett. 21 (1999) 83 4357.
[6] S. Nie, S.R. Emory, Probing single molecules and single nanoparticles by surface-enhanced Raman scattering, Science 275 (1997) 1102–1106.
[7] X. Wang, X. Zhu, H. Shi, Y. Chen, Z. Chen, Y. Zeng, Three-Dimensional-Stacked Gold Nanoparticles with Sub-5 Nm Gaps on Vertically Aligned TiO 2 Nanosheets for Surface-Enhanced Raman Scattering Detection Down to 10 fM Scale, vol. 10, 2018, pp. 35607–35614.
[8] X. Wang, X. Zhu, Y. Chen, M. Zheng, Q.Z.X. Tang, G. Zhang, H. Duan, Sensitive surface-enhanced Raman scattering detection using on-demand postassembled particle-on-film structure, ACS Appl. Mater. Interfaces 9 36 (2017), 31102.
[9] K. Kneipp, H. Kneipp, J. Kneipp, Acc. "Surface-Enhanced Raman scattering in local optical fields of silver and gold nanoaggregates from single-molecule Raman spectroscopy to ultrasensitive probing in live cells.", Acc. Chem. Res. 39 7 (2006) 443–450.
[10] M.M. Maye, J. Luo, L. Han, C.J. Zhong, Probing pH-tuned morphological changes in CoreShell nanoparticle assembly using atomic force microscopy, Nano Lett. 1 10 (2001) 575–579.
[11] A.M. Michaels, M. Nirmal, L.E. Brus, Surface enhanced Raman spectroscopy of individual rhodamine 6G molecules on large Ag nanocrystals, J. Am. Chem. Soc. 121 (1999) 9932–9939.
[12] T. Liu, Q. Liu, R. Hong, C. Tao, Q. Wang, H. Lin, Cuprous oxide induced the surface enhanced Raman scattering of silver thin films, Chem. Phys. Lett. 783 (2021) 783.
[13] X. Zhang, S. Zhang, C. Chang, Y. Feng, Y. Li, N. Dong, K. Wang, L. Zhang, W.J. Blau, J. Wang, Facile fabrication of wafer-scale MoS2 neat films with enhanced third-order nonlinear optical performance, Nanoscale 7 (2015) 2978–2986.
[14] Rostam Moradian, M. Saliminasab, Surface-enhanced Raman scattering in tunable bimetallic core-shell, Plasmonics 13 (2018) 1143–1151.
[15] Y. Yang, J. Shi, G. Kawamura, M. Nogami, Preparation of Au–Ag, Ag–Au core–shell bimetallic nanoparticles for surface-enhanced Raman scattering, Scripta Mater. 58 10 (2008) 862–865.
[16] B.N. Khlebtsov, Z. Liu, J. Ye, N.G. Khlebtsov, Au@Ag core/shell cuboids and dumbbells: optical properties and SERS response, J. Quant. Spectrosc. Radiat. Transf. 167 (2015) 64–75.

[17] J.M. Li, Y. Yang, D. Qin, Hollow nanocubes made of Ag-Au alloys for SERS detection with sensitivity of 108 M for melamine, J. Mater. Chem. C 2 (2014) 9934–9940.
[18] J. Ji, Z. Li, W. Sun, H. Wang, Surface plasmon resonance tuning in gold film on silver nanospheres through optical absorption, Sens. Bio-Sens. Res. (2020), 100374.
[19] R. Hong, X. Wang, J. Ji, C. Tao, D. Zhang, ITO induced tunability of surface plasmon resonance of silver thin film, Appl. Surf. Sci. 356 (2015) 701–706.
[20] P.B. Petrov, L. Barna, J. Hultman, E. Greene, Microstructural evolution during film growth, J. Vac. Sci. Techn. A-Vac. Sur. Films 21 (2003) S117–S128.
[21] R. Hong, W. Shao, W. Sun, C. Deng, C. Tao, D. Zhang, Laser irradiation induced tunable localized surface plasmon resonance of silver thin film, Opt. Mater. 77 (2018) 198–203.
[22] S. Guha, J. Yang, D.L. Williamson, Y. Lubianiker, J.D. Cohen, A.H. Mahan, Structural, defect, and device behavior of hydrogenated amorphous Si near and above the onset of microcrystallinity, Appl. Phys. Letters74 (1999) 1860–1862.
[23] E.W.H. Kan, W.K. Choi, C.C. Leoy, W.K. Chim, D.A. Antoniadis, E.A. Fitzgerald, Effect of annealing profile on defect annihilation, crystallinity and size distribution of germanium nanodots in silicon oxide matrix, Appl. Phys. Lett. (2003) 2058–2060.
[24] M. Ferraria, A.P. Carapeto, A. Rego, X-ray photoelectron spectroscopy: silver salts revisited, Vacuum 86 12 (2012) 1988–1991.
[25] D. Barreca, A. Gasparotto, C. Maragno, E. Tondello, Silica-supported Ag-Au bimetallic nanosystems by XPS, Surf. Sci. Spectra 13 1 (2006) 1, 0.
[26] G. Liu, Y. Liu, L. Tang, X. Liu, G. Fu, Z. Liu, Semiconductor-enhanced Raman scattering sensors via quasi-three-dimensional Au/Si/Au structures, Nanophotonics 8 (2019).
[27] Z. Huang, J. Chen, G. Liu, Y. Wang, Y. Liu, L. Tang, Thermally generated metals for plasmonic coloring and surface-enhanced Raman sensing, Opt. Eng. 57 3 (2018), 037103, 1-037103.5.
[28] S. Link, M.A. El-Sayed, Laser photothermal melting and fragmentation of gold nanorods: energy and laser pulse-width dependence, J. Phys. Chem. A 103 9 (1999) 1165–1170.
[29] N. Kometani, M. Tsubonishi, T. Fujita, K. Asami, Y. Yonezawa, Preparation and optical absorption spectra of dye-coated Au, Ag, and Au/Ag colloidal nanoparticles in aqueous solutions and in alternate assemblies, Langmuir 17 (2001) 578–580.
[30] Amit Bansal, S.S. Verma, Simulated study of plasmonic coupling in noble bimetallic alloy nanosphere arrays, AIP Adv. 4 5 (2014) 3094–3099.
[31] W. Wei, R. Hong, Y. Meng, C. Tao, D. Zhang, Electron-beam irradiation induced phase transformation, optical absorption and surface-enhanced Raman scattering of Indium tin alloy thin films, Superlattice. Microst. 106 (2017) 189–196.
[32] L. Lu, H. Wang, Y. Zhao, S. Xi, H. Zhang, J. Hu, B. Zhao, Seed-mediated growth of large, monodisperse core-shell gold-silver nanoparticles with Ag-like optical properties, Chem. Commun. 2 (2002) 144–145.
[33] N.R. Jana, L. Grearheart, C.J. Murphy, Wet chemical synthesis of silver nanorods and nanowires of controllable aspect ratio, Chem. Commun. 7 (2001) 617–618.
[34] E. Hao, G.C. Schatz, Electromagnetic fields around silver nanoparticles and dimers, Chem. Phys. 120 (2004) 357.
[35] R.G. Nikov, N.N. Nedyalkov, P.A. Atanasov, D. Hirsch, B. Rauschenbach, K. Grochowska, G. Sliwinski, Characterization of Ag nanostructures fabricated by laser induced dewetting of thin films, Appl. Surf. Sci. 374 (2016) 36–41.
[36] Aroca, F. Ricardo, Plasmon enhanced spectroscopy, Phys. Chemis. Chem. Phys.Pccp 15 15 (2013) 5355–5363.
[37] M. Fan, A.G. Brolo, Silver nanoparticles self-assembly as SERS substrates with near single molecule detection limit, Phys. Chem. Chem. Phys. 11 (2009) 7381–7389.